Hindawi
Advances in Materials Science and Engineering
Volume 2023, Article ID 8033881, 9 pages
https://doi.org/10.1155/2023/8033881

Research Article

Microfriction Stir Welding of Aluminium Using ABB IRB 1410 Robot

R. Manoj Samson,[1] **R. Aravind**,[1] **Solomon Jenoris Muthiya**,[2] **Joshuva Arockia Dhanraj**,[3] **Karthikeyan Velmurugan**,[4,5] **and Saw Lin Oo**[6]

[1]*Department of Mechanical Engineering, SRM Institute of Science and Technology, Kattankulathur, Chennai 603203, India*
[2]*Department of Automobile Engineering, Dayananda Sagar College of Engineering, Bengaluru, Karnataka 560078, India*
[3]*Centre for Automation and Robotics (ANRO), Department of Mechatronics Engineering, Hindustan Institute of Technology and Science, Padur, Chennai 603103, India*
[4]*Center for Alternative Energy Research and Development, Khon Kaen University, Khon Kaen, Thailand*
[5]*Mechanical Engineering Division, Faculty of Engineering, Khon Kaen University, Khon Kaen, Thailand*
[6]*Department of Physics & Universities' Research Centre, University of Yangon, Yangon, Myanmar*

Correspondence should be addressed to Solomon Jenoris Muthiya; jenoris.555@gmail.com and Saw Lin Oo; kosawlinoo@gmail.com

Received 7 August 2022; Revised 22 November 2022; Accepted 13 April 2023; Published 9 May 2023

Academic Editor: R. Thanigaivelan

Industry 4.0 industries are relying on automation processes using robots. Robots are multifunctional reprogrammable machines tuned to be used in any process with high accuracy and repeatability. The advent of intelligent technology allows better precision in the welding process. One such robotic welding process is the robot microfriction welding process which is slowly replacing conventional ones. Robot microfriction stir welding (RMFSW) process mainly relays on friction between the tool and material making it more suitable for joining metals in the industries such as automotive and aerospace applications. The robot-assisted MFSW process can provide better joints without human intervention. In this work, a shrinking flange has been designed and fabricated to grip the end effector with the robot. A microfriction stir welding tool was manufactured using EN24 and used to weld 1 mm thin aluminium 1100 sheets. Both the flange and MFSW tools were designed in SOLIDWORKS software. Taguchi *L9* was designed with three factors such as motor speed, traverse speed, and plunging depth. The robot microfriction stirs welded samples had controlled bead width and depth of penetration. Mechanical results show an improvement in hardness after the welding process. TOPSIS optimization technique was carried out. The motor speed of 20,000 rpm, traverse speed of 2 mm/sec, and plunge depth of 0.7 mm were found to be the best-optimized parameters.

1. Introduction

One of the unique challenges in producing compact products is the making of small and microcomponents. Especially, joining materials of 1000 μm or below it is a difficult process. This microjoining process can be achieved through highly accurate and precise automated robots. Micromanufacturing using industrial robots is possible by designing a special-purpose gripper tool for a particular process. One such microjoining process is microfriction stir welding (MFSW), which was developed in the welding institute by Wayne Thomas. It is an eco-friendly and solid-state welding process [1]. Solid-state welding is a process of joining two metals or alloys by producing friction between the tool and the base materials. The same method is followed in microfriction stir welding where the dimensions are reduced to a micron level. A tool made of a solid rod tougher than the base material is used in microfriction stir welding. The hard MFSW tool is made of a pin and shoulder that is to be rotated at greater velocity and simultaneously moved

through metals to join it by creating moderate heat and friction [2, 3]. Since MFSW is a solid-state process based on friction it produces low-level heat compared to other welding processes. It produces good-appearance welds with low distortion, at a relatively low cost. The only disadvantage of this technique has been its exit keyhole. MFSW is very useful in applications such as welding of complicated products like thin-walled structures, battery covers, and electrical and electronic components [4–6]. The μFSW process has four phases which is conducted in the order mentioned in Figure 1. Some of the principal process parameters of microfriction stir welding are the rotational speed of the tool, forward velocity of the tool and plunge depth. The torque or rotational force of the tool decides the frictional force between the tool and the material which transports the metal around the tool in the plastic zone. This parameter is important to produce the friction at the shoulder of the tool which gives the welding finish [7–9]. Traverse movement of the tool is essential to make the material move around the tool and move it forward. Plunge depth is decided by the thickness of the material. For example, for a sheet with a 1 mm thickness, the maximum plunge depth can be up to 0.9 mm [10]. It is very difficult to carry out fusion welding in a 1 mm sheet due to metallurgical problems and distortion. MFSW is utilized to carry out welding without distortion [11–13]. The disadvantage of the MFSW process is that it has a keyhole at the last stage, this technique is very scale-sensitive so high precision and accuracy are needed. The major advantage in the MFSW process compared to microresistance welding is that the joints are made at lower temperatures without any need of fluxes, gas, or consumable electrodes automatically reducing the risk of contamination or cleaning delicate components. This avoids the need of postwelding treatments which consequently reduces the welding cost. Mahidhar et al. has done TOPSIS optimization for laser-welded haste alloys [14].

The objective of this work is to carry out RMFSW process in aluminum 1100 using ABB IRB 1410 robot. In order to achieve the process a motor with high torque capacity is used as an end effector for the robot. A microfriction stir welding tool has been designed and manufactured in EN24 material. In this project, we are designing and manufacturing a special-purpose shrinking flange to grip the Makita RT0700C alternating current motor to the ABB IRB 1410 Project plan is shown in Figure 1. The aluminum 1100 is welded using RMFSW. The optimization of process parameters of the RMFSW was done using TOPSIS optimization.

2. Experimental Details

Aluminum 1100 alloy of 1 mm thin sheets with a dimension of $70 * 35$ mm was used throughout this study. The composition of Aluminium 1100 alloy is shown in Table 1.

2.1. Design of the Robotic Gripper. A special type of shrinking flange has been designed in SOLIDWORKS software and manufactured in H30 material to withhold the Makita RT0700C motor. Microfriction stir welding tool has been designed in SOLIDWORKS software and manufactured using EN24 material.

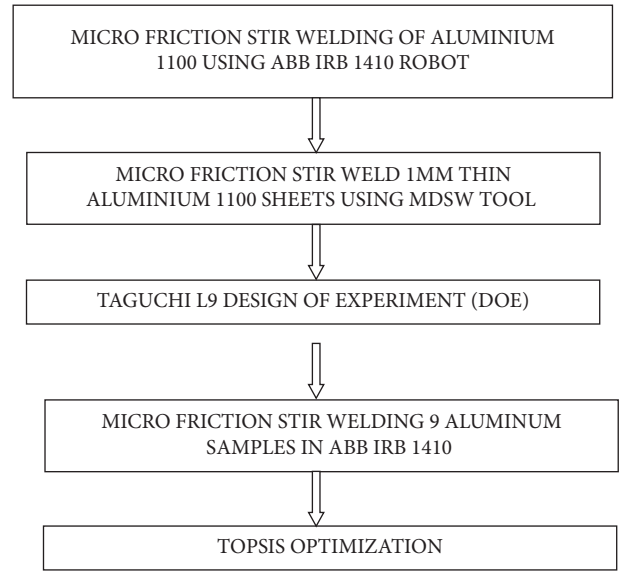

Figure 1: Robot microfriction stir welding.

2.2. Design of Backing Plate. The backing plate was designed in SOLIDWORKS to use in any type of welding process. It is manufactured in mild steel material and the whole setup is coated with blackening powder to prevent rust. The model is designed to act as a backing block and also as a shielding gas provider below the sheets. Turning it upside down it also can be used for RFSW process. The SOLIDWORKS design of the Backing plate is presented and the manufacturing block is presented in Figure 2.

2.3. Design of Microfriction Stir Welding Tool. The tool was designed in SOLIDWORKS software and the tool material was decided by considering workpiece material. In this work, aluminium 1100 alloy was chosen as a work piece material which has a hardness value of 144 HB. MFSW tool was selected based on a higher hardness value than the base material since our aluminum is a soft material. EN24 was chosen as MFSW tool with a hardness value of 248 HB. The tool was designed by considering the bending moment in the account so to reduce it a step-by-step cut design is used (Figure 3).

ABB IRB 1410 robot was used in this project to do the microfriction stir welding process with aid of Makita RT0700C AC motor and specially designed microfriction stir welding tool. The welding setup is shown in Figure 4.

The robot MFSW was done based on the *L9* Taguchi array by considering three levels of factors named as M = Motor speed (RPM), T = Traverse speed (mm/Sec) and P = Plunging depth (mm). Table 2 shows three levels of parameters with three factors.

The *L9* Taguchi design of the experiments table with both input and output parameters is mentioned in Table 3, where DOP, is the depth of penetration, and BW is bead width.

Table 1: Chemical composition of Al 1100 alloy.

Elements	Aluminium (Al)	Copper (Cu)	Iron (Fe)	Manganese (Mn)	Zinc (Zn)	Residuals
Components	99.0–99.95%	0.05–0.20%	0.95% max	0.05% max	0.1% max	0.15% max

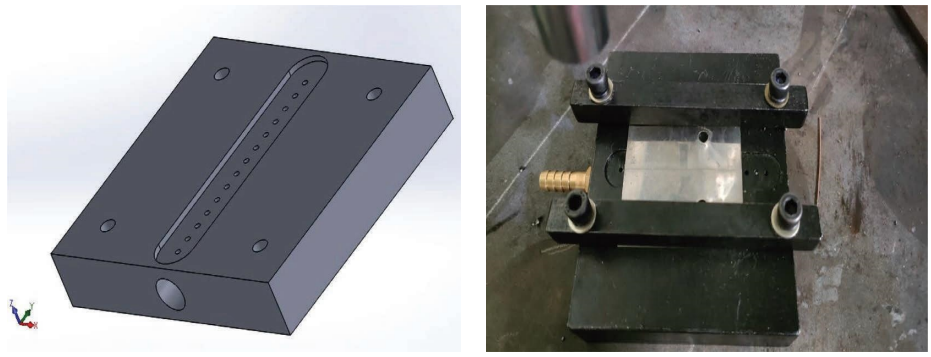

(a) (b)

Figure 2: Backing plate design solid works (a) and manufactured block (b).

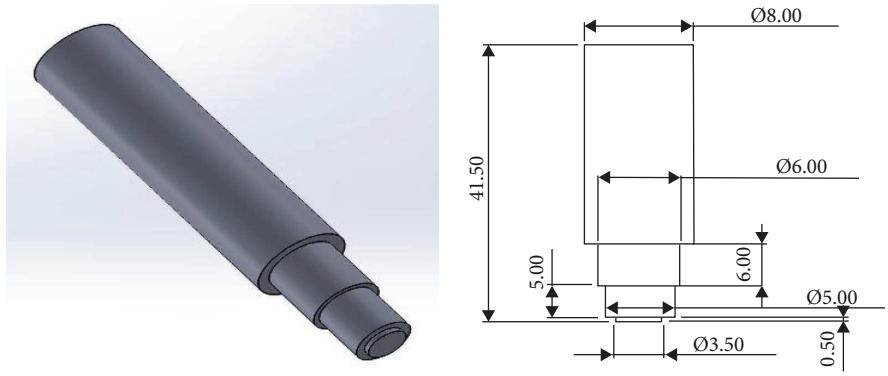

(a) (b)

Figure 3: Microfriction stir welding tool design (a) and tool dimensions (b).

The robot microfriction stir welded (RMFSW) 1 mm thin sheets of aluminium 1100 alloy sheets are shown in Figure 5.

After the RMFSW process, the welded specimen were cut down into 10 × 10 mm samples using the wire-EDM method and then cold-mounted. The cold-mounted samples were polished using emery sheets and the disc was polished using diamond paste. Further, the samples were etched using Keller's reagent [150 ml H_2O, 3 ml HNO_3, and 6 ml HF] for 20 seconds. Macrostructure was taken using a machine vision system and microhardness testing was carried out in a micro-Vickers hardness tester with the model number of HMV-G made by Shimadzu.

3. Results and Discussion

3.1. Macrostructure. The macrostructure of the welded samples is taken from the machine vision system. BW and DOP of the samples are measured using VMS 3.1 software. Measured values are tabulated below. All the samples have achieved a bead width of 3.5 mm approximately and the samples have achieved the applied depth of penetration with a variation of ±0.02 mm. Sample images are revealed in Figure 6 and (see Tables 4 and 5).

3.2. Microhardness. Microhardness test was carried out in Vickers hardness tester. The values are taken in the interval of 10 mm on either side of the weld zone and on the weld zone. The average microhardness values of the welded samples are tabulated below. Samples 7, 8, and 9 had the highest hardness of 43 HV.

3.3. Optimization (TOPSIS). TOPSIS stands to be a technique for order preference by similarity to the ideal solution which is a common technique that has been used in automobile industries for decision making. This technique has six stages as follows:

Stage I: Determination of a Performance Matrix

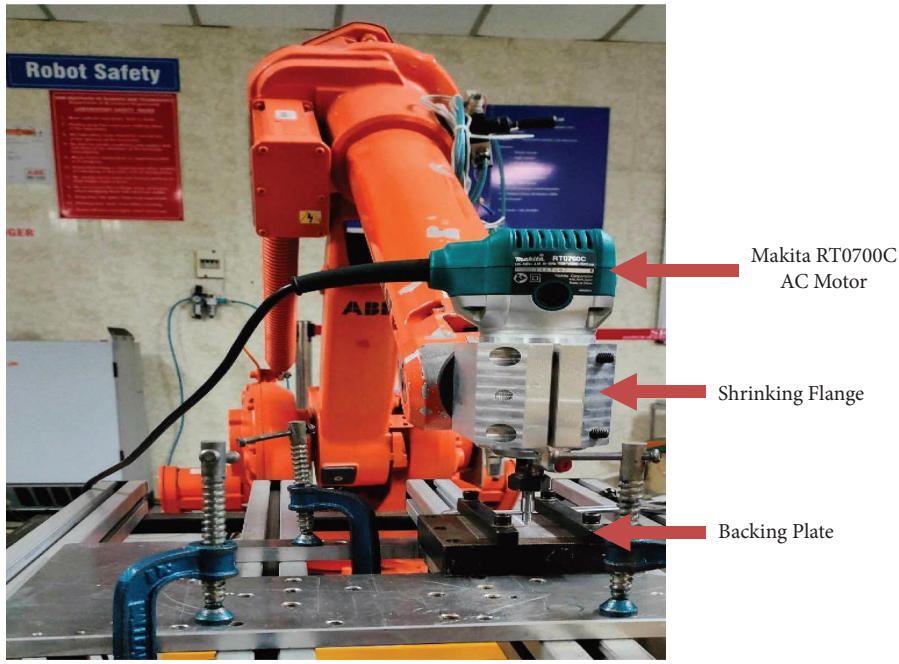

Figure 4: Robot microfriction stir welding setup.

Table 2: Level of parameters.

Factors	*L*1	*L*2	*L*3
M (RPM)	10,000	16,000	20,000
T (mm/Sec)	1	2	3
P (mm)	0.5	0.6	0.7

Table 3: *L9* input and output parameters.

	Input parameters			Output parameters		
Sample no	Motor speed (RPM)	Traverse speed (mm/Sec)	Plunging depth (mm)	DOP (mm)	BW (mm)	Hardness (Hv)
1	10000	1	0.5	0.4989	3.48	42.3
2	10000	2	0.6	0.602	4.42	42
3	10000	3	0.7	0.7233	4.45	42
4	16000	1	0.6	0.5936	4.43	41.3
5	16000	2	0.7	0.7103	4.48	42.6
6	16000	3	0.5	0.4852	3.47	42.3
7	20000	1	0.7	0.7713	4.45	43
8	20000	2	0.5	0.4731	3.43	43.3
9	20000	3	0.6	0.584	4.49	43.3

Stage II: Calculation of Normalized Decision Matrix

Stage III: Calculate Weighted Normalized Decision Matrix

Stage IV: Determination of the Ideal (D_i^+) and (D_i^-)

Stage V: Calculate the Euclidian Distance between Ideal (D_i^+) and Ideal (D_i^-)

Stage VI: Determine the Relative Performance Closeness to the Ideal Soln.

In this project, depth of penetration and hardness is considered to be larger the better criteria whereas bead width is considered to be smaller the better criteria.

Stage I: Determination of a Performance Matrix

Calculate the sum of squares for DOP, BW, and microhardness to calculate the performance matrix. The performance matrix of the above-mentioned parameters is shown in Table 6.

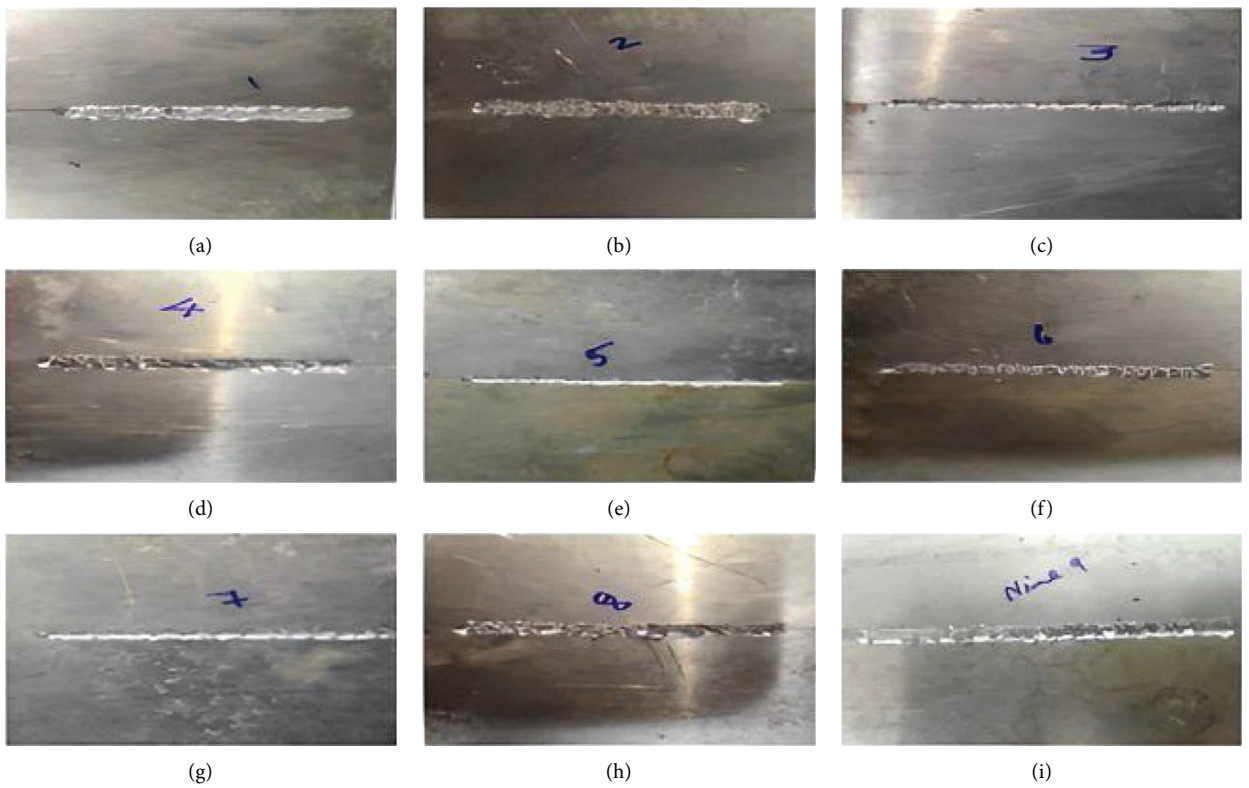

(a) (b) (c)

(d) (e) (f)

(g) (h) (i)

Figure 5: Robot microfriction stir welded *L*9 samples.

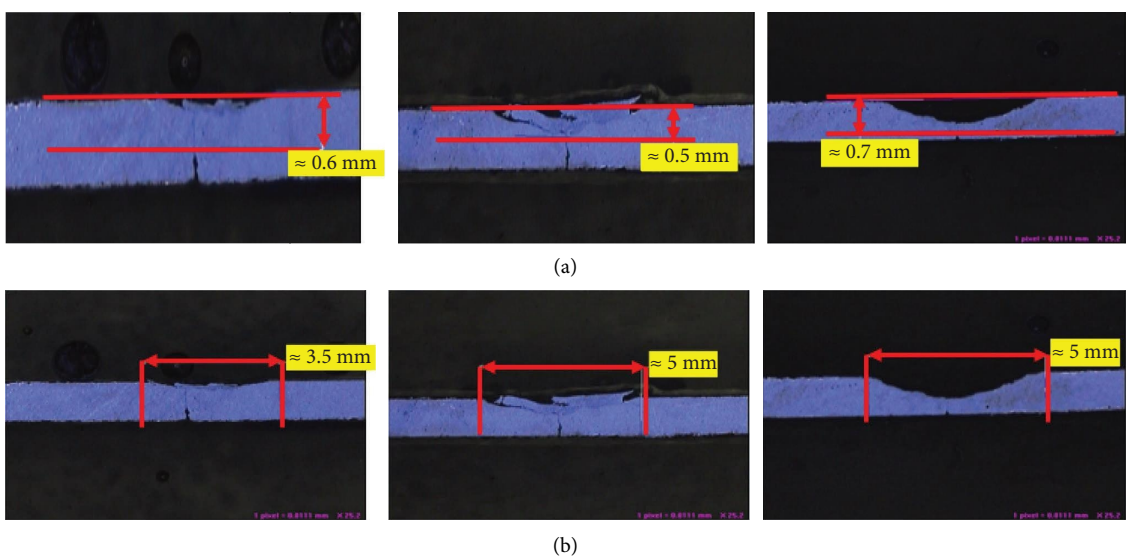

Figure 6: MFSW samples macrostructure: (a) depth of penetration and (b) bead width.

Table 4: DOP and BW of MFSW samples.

Sample no	DOP (mm)	BW (mm)
1	0.4989	3.48
2	0.602	4.42
3	0.7233	4.45
4	0.5936	4.43
5	0.7103	4.48
6	0.4852	3.47
7	0.7713	4.45
8	0.4731	3.43
9	0.584	4.49

Table 5: Microhardness of welded samples.

Sample no	Hardness (Hv)
1	42.3
2	42
3	42
4	41.3
5	42.6
6	42.3
7	43
8	43.3
9	43.3

Table 6: Performance matrix.

Sample no	DOP (mm)	BW (mm)	Hardness (Hv)
1	0.4989	3.48	42.3
2	0.602	4.42	42
3	0.7233	4.45	42
4	0.5936	4.43	41.3
5	0.7103	4.48	42.6
6	0.4852	3.47	42.3
7	0.7713	4.45	43
8	0.4731	3.43	43.3
9	0.584	4.49	43.3
SOS	**3.386557**	**154.913**	**16225.81**

Bold value is the maximum threshold of the values.

Stage II: Calculation of Normalized Decision Matrix

Equation (1) is used to calculate Normalized Decision Matrix. Table 7 shows the corresponding values.

$$U_{ij} = \frac{x_{ij}}{\sqrt{\left(\sum x_{[i]j}^2\right)}}. \quad (1)$$

Stage III: Calculate Weighted Normalized Decision Matrix

Weights are allocated to output parameters based on optimization techniques. Weights are distributed equally in percentage to the input parameters. So, 0.35, 0.3, and 0.35 has been selected as equal percentage weight for the input parameters. Corresponding values are mentioned in Table 8 and the matrix is shown in Table 9.

We can calculate the weighted normalized matrix,

$$B_{ij} = M_{ij} \times N_{ij}. \quad (2)$$

Stage IV: Determination of the Ideal (D_i^+) and (D_i^-)

Table 10 reveals ideal worst and best numbers.

Ideal Positive Soln. = P_j^+ (min or max).

Ideal Negative Soln. = P_j^- (min or max).

Stage V: Calculate the Euclidian Distance between Ideal (D_i^+) and Ideal (D_i^-)

Euclidian Distance values calculated using equations (3) and (4) are shown in Table 11.

Table 7: Normalized decision matrix.

Sample no	DOP (mm)	BW (mm)	Hardness (Hv)
1	0.271103	0.279599	0.332076
2	0.327128	0.355123	0.329721
3	0.393042	0.357533	0.329721
4	0.322563	0.355926	0.324225
5	0.385978	0.359943	0.334431
6	0.263658	0.278795	0.332076
7	0.419126	0.357533	0.337571
8	0.257083	0.275582	0.339926
9	0.317346	0.360747	0.339926

Table 8: Weighted matrix.

Depth of penetration (mm)	Bead width (mm)	Hardness (Hv)
0.35	0.3	0.35

Table 9: Weighted normalized decision matrix.

Sample no	DOP (mm)	BW (mm)	Hardness (Hv)
1	0.094886	0.08388	0.116227
2	0.114495	0.106537	0.115402
3	0.137565	0.10726	0.115402
4	0.112897	0.106778	0.113479
5	0.135092	0.107983	0.117051
6	0.09228	0.083639	0.116227
7	0.146694	0.10726	0.11815
8	0.089979	0.082674	0.118974
9	0.111071	0.108224	0.118974

Table 10: Determination of ideal (D_i^+) and ideal (D_i^-).

	DOP (mm)	BW (mm)	Hardness (Hv)
B+	0.146694	0.082674	0.118974
B–	0.089979	0.108224	0.113479

Table 11: Euclidian distance between ideal (D_i^+) and ideal (D_i^-).

Sample no	E_i^+	E_i^-
1	0.051895	0.024985522
2	0.040236	0.024648703
3	0.026468	0.047634276
4	0.041874	0.02296354
5	0.027907	0.045255018
6	0.054491	0.024845285
7	0.024599	0.056915002
8	0.056715	0.02613385
9	0.043838	0.021796252

Table 12: Relative performance closeness to ideal solution.

Sample no	Pi	Rank
L1	0.324993	7
L2	0.379883	4
L3	0.642820	2
L4	0.354173	5
L5	0.618556	3
L6	0.313163	9
L7	0.698222	1
L8	0.315441	8
L9	0.332087	6

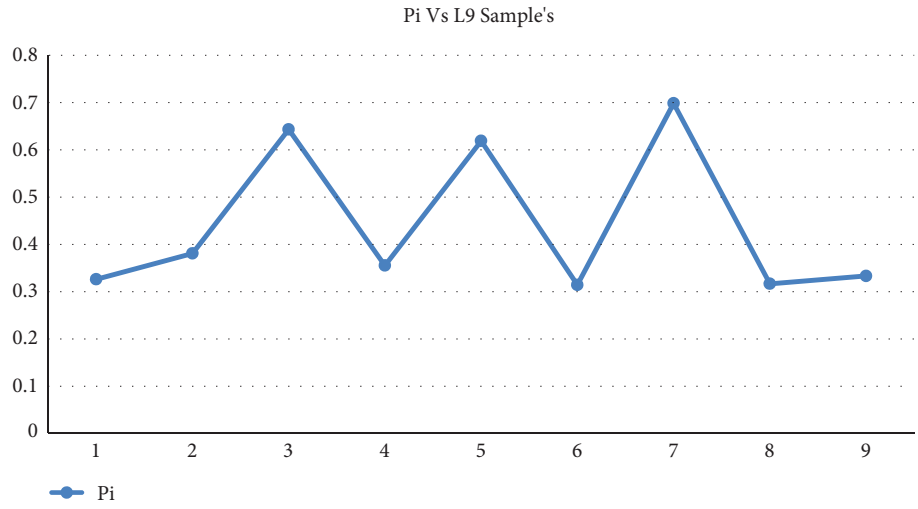

Figure 7: Pi vs. *L9* samples.

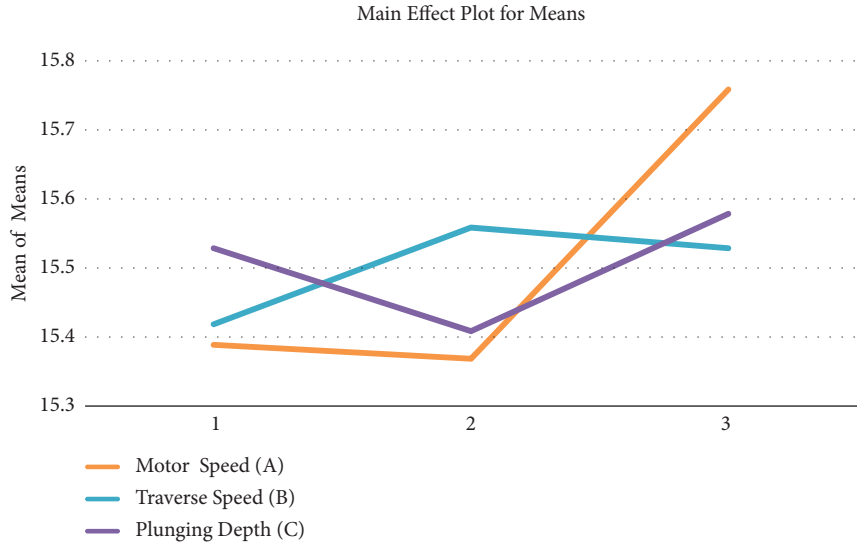

Figure 8: Main effect plot of input parameters.

Table 13: Response table.

Level	Motor speed (A)	Traverse speed (B)	Plunging depth (C)
1	15.39	15.42	15.53
2	15.37	**15.56**	15.41
3	**15.76**	15.53	**15.58**
Delta	0.38	0.13	0.16
Rank	1	3	2

Bold value is the maximum speed attained.

Table 14: Optimized parameter combination.

Factors	Initial values	Optimized parameters	
Setting level	$A_1\ B_1\ C_1$	Prediction $A_3\ B_2\ C_3$	Experiment $A_3\ B_2\ C_3$
DOP (mm)	0.4989	—	0.70012
BW (mm)	3.48	—	3.5
Hardness (HV)	42.3	—	43.3
Pi	0.324993	0.402025	0.410251

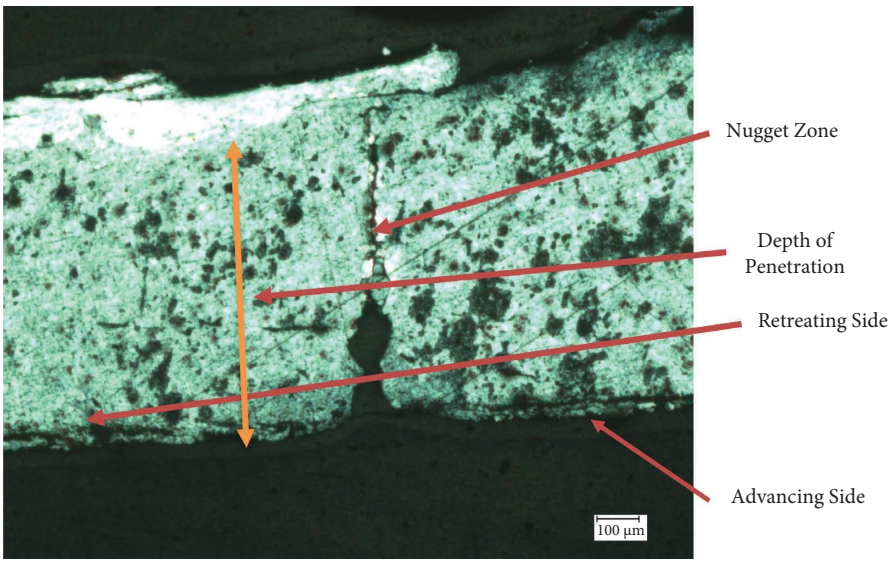

Figure 9: Microstructure of optimized sample.

$$E_i^+ = \left[\sum \left(D_i^+ - B_{ij}\right)^2\right]^{0.5}, \tag{3}$$

$$E_i^- = \left[\sum \left(D_i^- - B_{jj}\right)^2\right]^{0.5}. \tag{4}$$

Stage VI: Determine the Relative Performance Closeness to the Ideal Soln.

$$P_i = \frac{E_i^-}{E_i^+ + E_i^-}. \tag{5}$$

Table 12 reveals relative performance closeness and its rank.

Figure 7 shows graphical representation of Pi (closeness value) vs. $L9$ samples.

3.3.1. Response Value Table Using Closeness Value. $A_3\ B_2\ C_3$ was found to be the best optimal parameter in the Taguchi $L9$. Motor speed had the highest influence on input parameters followed by plunge depth and traverse speed, respectively. Figure 8 shows the best optimal level of the parameter (see Table 13).

The mean line was found around 15.5 above this point all the input good results but our optimal level was found to be out of $L9$ so a confirmatory test was done.

3.3.2. Confirmation Test. In order to find the optimized parameter set Pi value was predicted using the following equation:

$$[ee] = h_{m+} \sum (h - h_m), \tag{6}$$

where h_m average of Pi values, h is the mean of Pi values at the optimum level. The optimized parameters are presented in Table 14.

The experiment was done again using predicted values and the optimal parameter combination is found with DOP = 0.7 mm; BW = 3.5 mm; and hardness = 43.3 HV. Figure 9 shows the microstructure of the optimized parameter.

4. Conclusion

(1) Robot microfriction stir welding (RMFSW) of 1 mm thin aluminum 1100 sheets was successfully done using ABB IRB 1410 robot.

(2) *L*9 Taguchi was designed with three factors and three levels.

(3) In microstructure analysis, the weld zone had a fine grain structure, which increases the hardness value of the material.

(4) Microhardness seemed to be higher after the welding process which has increased up to 43.3 HV.

(5) In TOPSIS sample number 7 had the highest rank compared to all other samples. Sample 7 has input parameters such as motor speed = 20000 rpm; traverse speed = 1 mm/sec; and depth of penetration = 0.7 mm. It had a dop of 0.7 mm; a bead width of 3.45; and a hardness of 43 HV.

(6) A confirmation test was carried out and $A_3B_2C_3$ was found to be the best optimal input parameter.

(7) Motor speed is found to be the most influencing parameter among all three, succeeded by plunge depth and traverse speed, respectively.

Data Availability

The data used to support the findings of this study are made available from the corresponding author upon request.

Conflicts of Interest

The authors declare that they have no conflicts of interest.

References

[1] M. Simoncini, D. Ciccarelli, A. Forcellese, and M. Pieralisi, "Micro-and macro-mechanical properties of pinless friction stir welded joints in AA5754 aluminium thin sheets," *Procedia Cirp*, vol. 18, pp. 9–14, 2014.

[2] B. T. Gibson, D. H. Lammlein, T. J. Prater et al., "Friction stir welding: process, automation, and control," *Journal of Manufacturing Processes*, vol. 16, no. 1, pp. 56–73, 2014.

[3] K. Wang, F. Léonard, and G. Abba, "Dynamic model identification of axial force in robotic friction stir WeldingÕ," *IFAC-PapersOnLine*, vol. 48, no. 3, pp. 1936–1941, 2015.

[4] M. Guillo and L. Dubourg, "Impact & improvement of tool deviation in friction stir welding: weld quality & real-time compensation on an industrial robot," *Robotics and Computer-Integrated Manufacturing*, vol. 39, pp. 22–31, 2016.

[5] J. Qin, F. Léonard, and G. Abba, "Real-time trajectory compensation in robotic friction stir welding using state estimators," *IEEE Transactions on Control Systems Technology*, vol. 24, no. 6, pp. 2207–2214, 2016.

[6] K. Sithole and V. V. Rao, "Recent developments in micro friction stir welding: a review," *IOP Conference Series: Materials Science and Engineering*, vol. 114, no. 1, Article ID 012036, 2016, February.

[7] Y. Huang, X. Meng, Y. Zhang, J. Cao, and J. Feng, "Micro friction stir welding of ultra-thin Al-6061 sheets," *Journal of Materials Processing Technology*, vol. 250, pp. 313–319, 2017.

[8] J. A. Joy, M. Sajjad, and D. W. Jung, "Design and fabrication of friction stir welding machine," in *MATEC Web of Conferences*, vol. 207, EDP Sciences, Article ID 03022, 2018.

[9] Y. Sagheer-Abbasi, S. Ikramullah-Butt, G. Hussain, S. H. Imran, A. Mohammad-Khan, and R. A. Baseer, "Optimization of parameters for micro friction stir welding of aluminum 5052 using Taguchi technique," *The International Journal of Advanced Manufacturing Technology*, vol. 102, no. 1-4, pp. 369–378, 2019.

[10] H. Luo, J. Fu, L. Jiao, G. Liu, C. Yu, and T. Wu, "KiNematics and dynamics analysis of a new-type friction stir welding robot and its simulation," *Advances in Mechanical Engineering*, vol. 11, no. 7, Article ID 168781401986651, 2019.

[11] K. N. Salloomi, F. I. Hussein, and S. N. Al-Sumaidae, "Temperature and stress evaluation during three different phases of friction stir welding of AA 7075-T651 alloy," *Modelling and Simulation in Engineering*, vol. 2020, Article ID 3197813, 11 pages, 2020.

[12] M. Sen, S. Shankar, and S. Chattopadhyaya, "Micro-friction stir welding (μFSW)–A review," *Materials Today: Proceedings*, vol. 27, pp. 2469–2473, 2020.

[13] P. Zolghadr, M. Akbari, and P. Asadi, "Formation of thermomechanically affected zone in friction stir welding," *Materials Research Express*, vol. 6, no. 8, Article ID 086558, 2019.

[14] V. Mahidhar, K. R. Sampreet, R. Kannan, and T. D. B. Kannan, "Parameter optimization in laser welding of Hastelloy C-276 using TOPSIS," *Materials Today: Proceedings*, vol. 21, pp. 595–600, 2020.